AIAA-2003-4181

VOLUMETRIC NEAR-FIELD MICROWAVE PLASMA GENERATION

R. J. Exton, R. Jeffrey Balla, and G. C. Herring
NASA Langley Research Center
Hampton, VA 23681

S. Popović and L. Vušković
Department of Physics, Old Dominion University
Norfolk, VA 23508

Abstract

A periodic series of microwave-induced plasmoids is generated using the outgoing wave from a microwave horn and the reflected wave from a nearby on-axis concave reflector. The plasmoids are spaced at half-wavelength separations according to a standing-wave pattern. The plasmoids are enhanced by an "effective focusing" in the near field of the horn (Fresnel region) as a result of a diffractive narrowing. Optical imaging, electron density, and rotational temperature measurements characterize the near field plasma region. Volumetric microwave discharges may have application to combustion ignition in scramjet engines.

A. Introduction

This paper presents an overview of a series of laboratory experiments with volumetric plasmas generated by a pulsed microwave radiation using a Ku-band (9.5 GHz) or an X-band (16.5 GHz) generator. The purposes of present experiments were to characterize the plasma generated near the bow shock in previous [1] Mach 6 experiments and to investigate various possibilities for extending similar plasmas off board (detached from nearby surfaces) for applications to supersonic combustion ignition. The present report focuses on the phenomenological characterization of the standing wave plasmoids generated around the local interference maxima of the microwave interference pattern.

Characterization of the plasma included determination of rotational and vibrational temperature and their dependence on pressure, position, power, and other microwave parameters. Validity of rotational and vibrational temperature data as qualitative indicators for gas temperature and microwave energy deposition in the ionized gas is addressed in a separate analysis (section D). Rotational temperature was determined from the (0-2) band of the $C^3\Pi_u \rightarrow B^3\Pi_g$ Second Positive System of molecular nitrogen. The effective vibrational temperature was determined by the detailed analysis of most band sequences of the Second Positive System (SPS) of N_2. In subsequent paragraphs, the results of the analysis and the issues related to the various techniques are discussed in detail. Special attention is given to the determination of electron density, which is the important parameter that controls the microwave radiation transfer to the discharge. In plasma structures with a low degree of ionization, a relationship between the electron density and emission intensity from the (0-0) band at 337.13 nm from the Second Positive System of molecular nitrogen was used to estimate space variation of electron density [2,3].

B. Apparatus

Experimental work was conducted in a static plasma cell, shown in fig. 1. The photo of the laboratory cell shows the position of the model containing the microwave horn and the concave reflector (removable for end-on observations). The cell was evacuated to the background air pressure in the same range as the static pressure in our Mach 6 tunnel experiment [1]. The same model that was used in the wind tunnel experiment was placed inside the cell, together with a concave metal reflector to form a linear microwave cavity. The model contained a microwave horn antenna whose aperture was covered with a ceramic plate.

The plasma was observed in two arrangements: *end-on,* parallel to the axis of the horn and microwave beam, and *side-on,* parallel to the surface of the horn, which are both shown schematically in fig. 2. This approach was motivated by possible existence of self-absorption effects in the preliminary side-on observations, which could distort the rotational band spectra. The microwave generation apparatus is described in ref. [1].

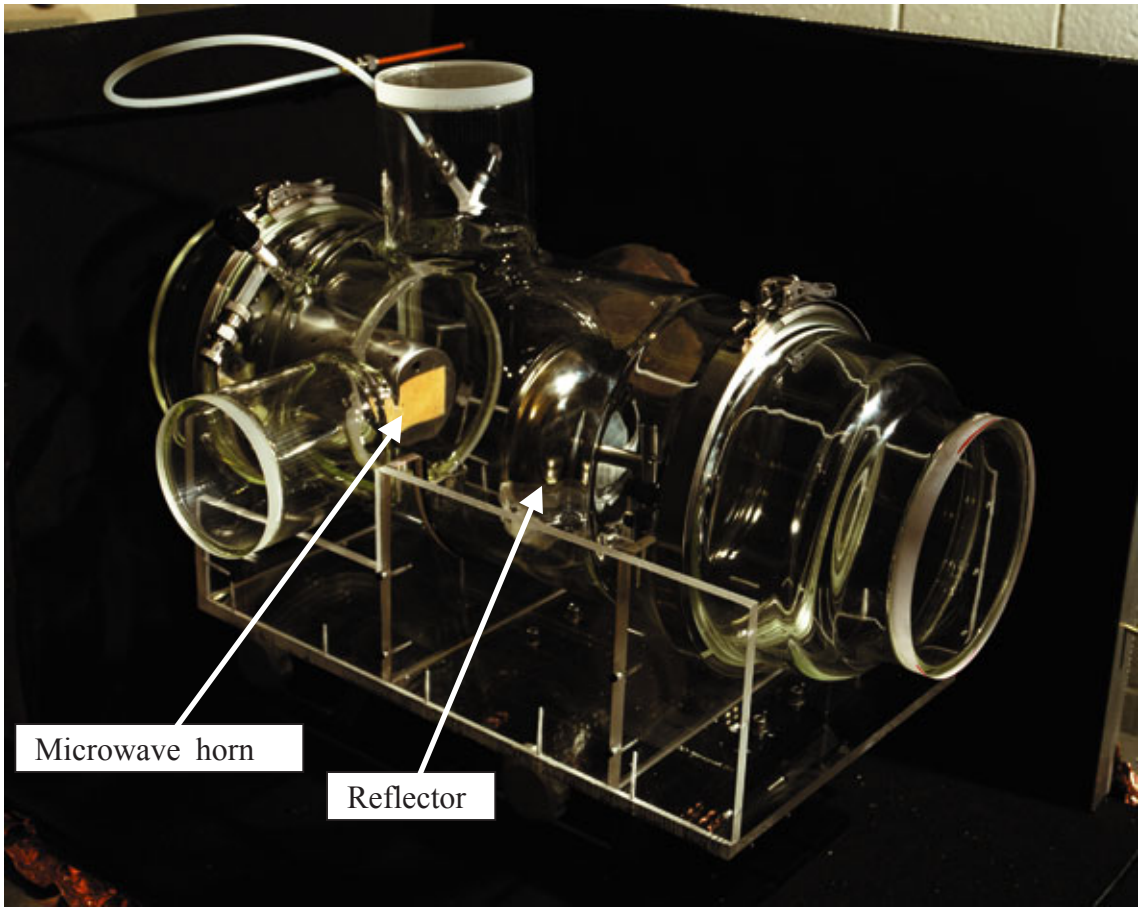

Fig. 1. Laboratory cell showing the model (microwave horn) and the concave reflector.

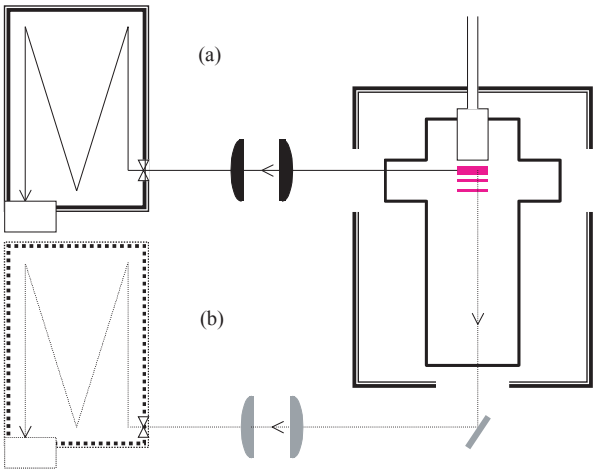

Fig. 2. Imaging spectrometer arrangement for (a) side-on and (b) end-on observations.

Emission spectra were recorded using a 0.5-m Acton Research Corporation imaging spectrograph with a 3600 g/mm grating blazed at 240 nm, an 1800 g/mm grating blazed at 500 nm, or a 600 g/mm grating blazed at 300 nm. The detection system consisted of an Apogee spectral imaging camera with a Hamamatsu CCD detector (1024 × 256 pixels) or a Tektronix CCD detector (512 × 256 pixels). A second camera, a Stanford Computer Optics, Inc., model 4 QUIK O5A, was used to observe the plasma in gated format with a time resolution of 50 ns. Alternatively, transient signals at fixed wavelengths were recorded using a photomultiplier tube.

Linear response within the dynamic range of the CCD arrays was verified in a series of tests with quartz neutral filters at several wavelengths across the spectral range (300–700 nm) used in diagnostics. Because the recorded spectra were integrated from a train of radiation pulses at a repetition rate typically about 100 pps, the dynamic range could be expanded over several orders of magnitude by variation of integration time. During this type of measurement, the reproducibility of recorded intensity was verified at every change of integration time.

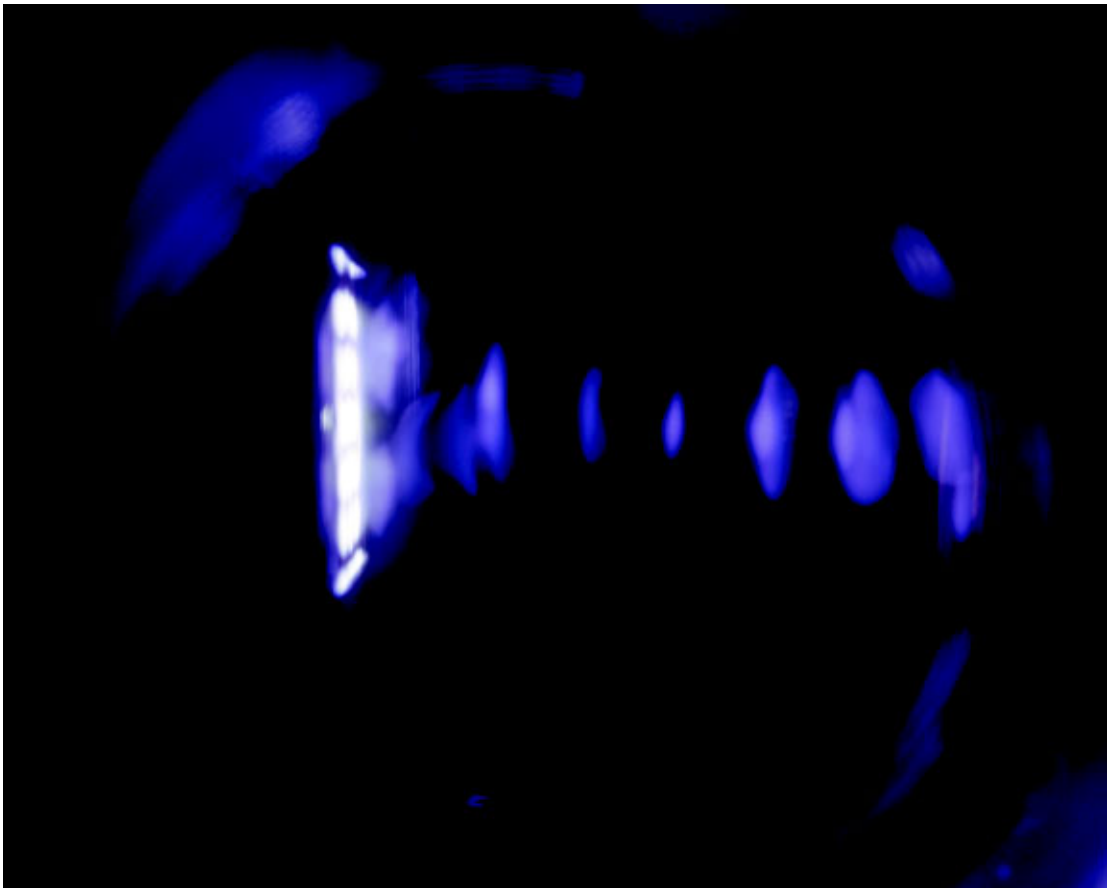

Fig. 3. Side view of the standing-wave plasmoids (X-band) produced using the concave reflector.

C. Visual Effects

C.1. Breakdown

Two frequency bands, X and Ku, are most easily identified by the microwave breakdown characteristics. For traveling wave conditions at a pressure of 10 torr, the power flux density necessary for microwave breakdown is about three times smaller for the X-band than for the Ku-band. This difference between band characteristics was immediately observed in the present work.

The discharge was more difficult to trigger with Ku-band than with the X-band. Addition of an external radiation source in order to generate seed electrons for breakdown was contemplated in the beginning of this work. However, addition of water vapor into the cell has solved most breakdown problems.

With the X-band generator, the breakdown was easily accomplished without external electron source or addition of water vapor. Because X-band has a substantially lower frequency, the discharge could be triggered at 30 torr, compared with about 10 to 15 torr in the case of Ku-band.

C.2. Discharge Structure

As shown in fig. 3, the discharge consisted of a bright planar plasma layer at the surface (a few millimeters thick) followed by the train of disc- and cone-shaped plasmoids spaced equidistantly at about half a wavelength apart. A dim funnel-shaped glow (proboscis) which is not visible in fig. 3, filled the space between plasmoids and followed the assumed trace of the microwave beam. A similar plasmoid structure was discussed in ref. [4].

At the horn aperture, the field amplitude pattern had multiple maxima, corresponding to the number of half-wavelength nodes over the width of the horn. These maxima are responsible for the structure of surface discharge with the luminous pattern that is seen in fig. 4. The discharge was generated in air at 17 torr using an X-band microwave pulse of duration 3.5 μs, power 210 kW, and repetition rate of 30 pps.

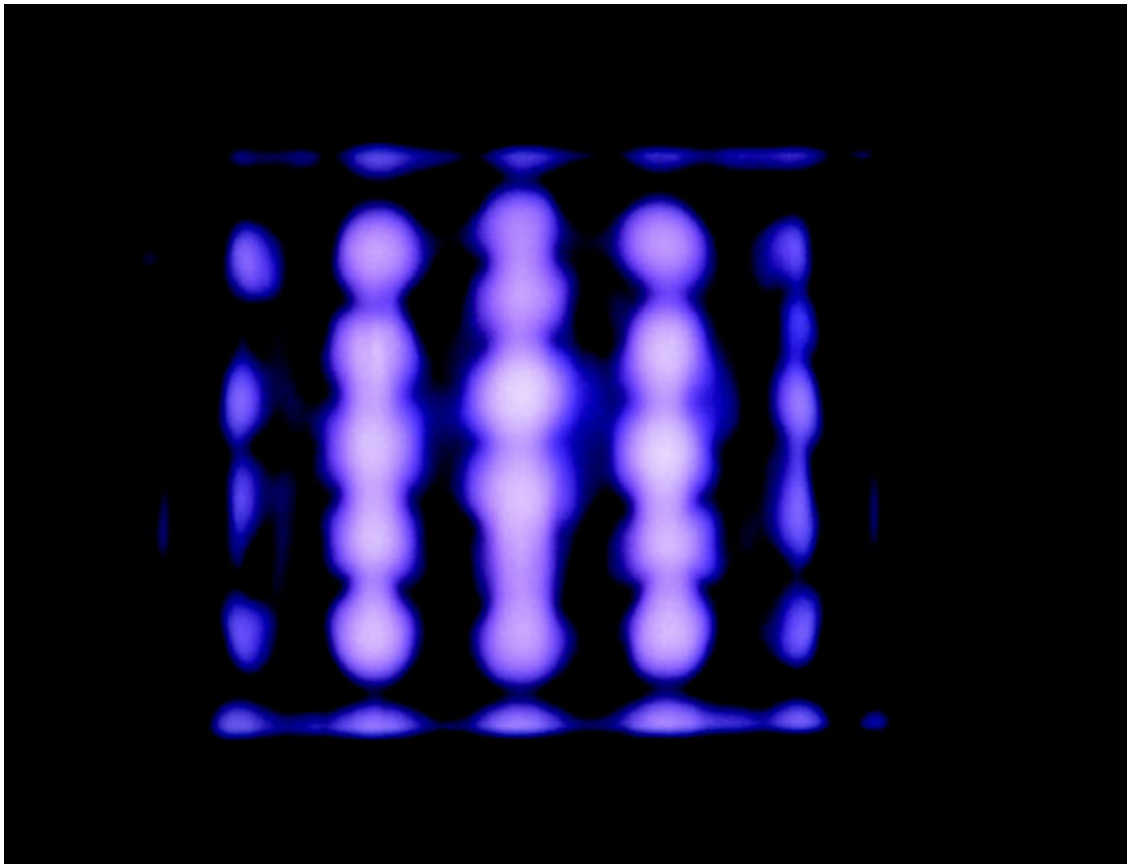

Fig. 4. End-on view of the surface plasma (X-band).

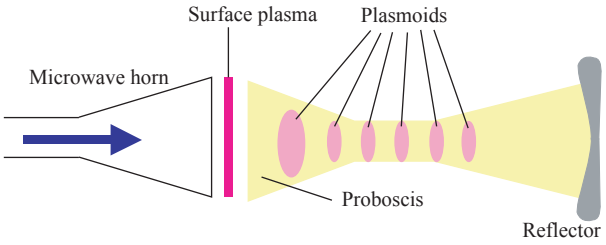

Fig. 5. Schematic view of volumetric plasma formations.

The visual image of the full pattern that consists of the surface plasma, the dim proboscis, and the plasmoids, shown schematically in fig. 5, depends on the repetition rate, pulse duration, power, and pressure. It was most clearly seen between 30 and 50 torr. At higher repetition rates, the neck of the proboscis appears narrower and a smaller number of plasmoids was observed. In the presence of water, plasmoids are visible only at the longest pulse duration. The discharge pattern changes with pulse power and frequency.

In the end-on observation at stable conditions and at relatively low pressure, the surface discharge assumes a symmetric pattern of bright and dark spots (see fig. 4). The pattern observed in the surface discharge is the consequence of near-field transformation of the physical characteristics of the wave due to diffraction. In the transition region between the Fresnel and Fraunhofer regimes, the cross section of the beam could be transformed into a double-maximum distribution, as shown in fig. 6 [5]. The double-maximum pattern then transforms to a narrow single maximum. In the far field, the single-maximum distribution changes to a broad single maximum that expands at the divergence angle of the horn.

During the excitation with X-band, an oxygen-rich mixture at 50 torr showed surface discharge with a similar pattern as in the case of excitation with Ku-band. Several plasmoids were observed at positions of the standing-wave maximums. The surface plasma and plasmoids appear violet, suggesting mostly nitrogen emission. In the background along the microwave

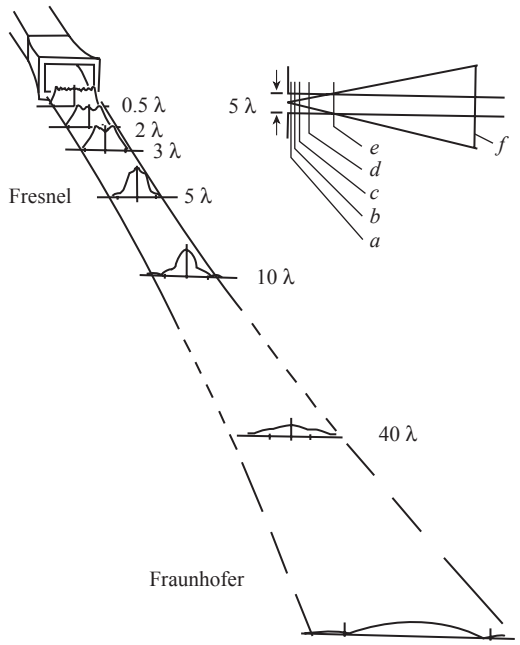

Fig. 6. Diffraction pattern (1-D) of microwave beam.

beam, the proboscis, glowing yellow-green, had the form of a funnel (see fig. 7). This dim glow was named proboscis for its protrusion into the free space. The glow followed the expected shape of the diffraction pattern. It had a wider cross section near the horn, the narrow neck-like region at about 2 to 3 wavelengths from the horn's aperture plane, and a conical shape toward the end window. The proboscis was brighter immediately behind the surface plasma. In an oxygen-rich mixture the diffuse glow was much more pronounced, stretching along the full length of microwave beam inside the cell. It obtained yellow-green color, which suggested the main mechanism for the glow to be the chemiluminescence during formation of NO_x from NO [6]. When the oxygen was blown into the cell, the dim glow moved around, apparently deflected by the flow. The current interpretation is that the proboscis appears as a signature of the intensive chemiluminescence. The pattern follows the oxygen-rich region and changes position in the flow. The presence of substantial electron density in this region is verified by a relatively strong emission from the bands belonging to both the First Negative and the Second Positive Systems. Neither the nitrogen molecular ion nor the electronically excited neutral molecule could be present in such abundance without the presence of electrons. Other researchers [7,8] also observed a formation similar to the proboscis and named it "aureole." They suggest an alternative possibility that aureole is the photoionization plasma generated by VUV radiation from the filamentary plasma in high-pressure microwave discharges.

The chemiluminescent signature of the proboscis, a broadband continuum of NO_x spread over the whole visible range, may be the background continuum observed with a low-resolution grating (see fig. 8). The indicated bandheads are, from left to right, (2,7), (1,6), (4,10), (0,5), (3,9), (2,8), (1,7), and (0,6) emission bands of the Second Positive System of molecular nitrogen. The spectrum was generated in room air at 30 torr enriched with oxygen. The X-band parameters were: pulse power 205 kW, duration 3.5 μs, and a repetition rate of 88 pps. However, the presence of (1-0), (0-0), and many other bands of the Second Positive System was observed in the spectrum of the proboscis, suggesting the presence of electrons probably came from photoionization. Although a relative contribution of the two mechanisms is not quite clear, they both contribute—one directly, the other indirectly—to weak volumetric ionization in the proboscis region.

Preliminary tests with oxygen have shown that using the oxygen-rich mixture may be an approach for coupling more energy into the gas. More oxygen leads to a decrease of the electron density and the reflectance of the surface plasma. Thus, more microwave power propagates into the cell. A quantitative estimate of the redistribution of the absorbed power is difficult to make.

All of the above observations were consistent with the expected volumetric, near-field distribution of the microwave field intensity, which was combined with the effect of the standing-wave pattern of the linear cavity. The near-field (Fresnel) pattern of the microwave beam has the "effective focusing" property as illustrated in fig. 6. In the far-field (Fraunhofer) regime, the diffraction effects fade away, and the beam takes the better-known profile with a divergence angle defined by the geometry of the horn.

In a series of tests the reflector was removed from the cell and an absorber was positioned near the end window. In dry air, a faint proboscis and at least one plasmoid was observed, even when the absorber was placed at an angle to the beam axis. However, in the artificially moistened air, the proboscis and plasmoids disappeared.

Another test with a reflector in the cell and X-band generation has shown a promising result. At about 70 torr, with the addition of oxygen, the electric field level at the aperture was not high enough to produce

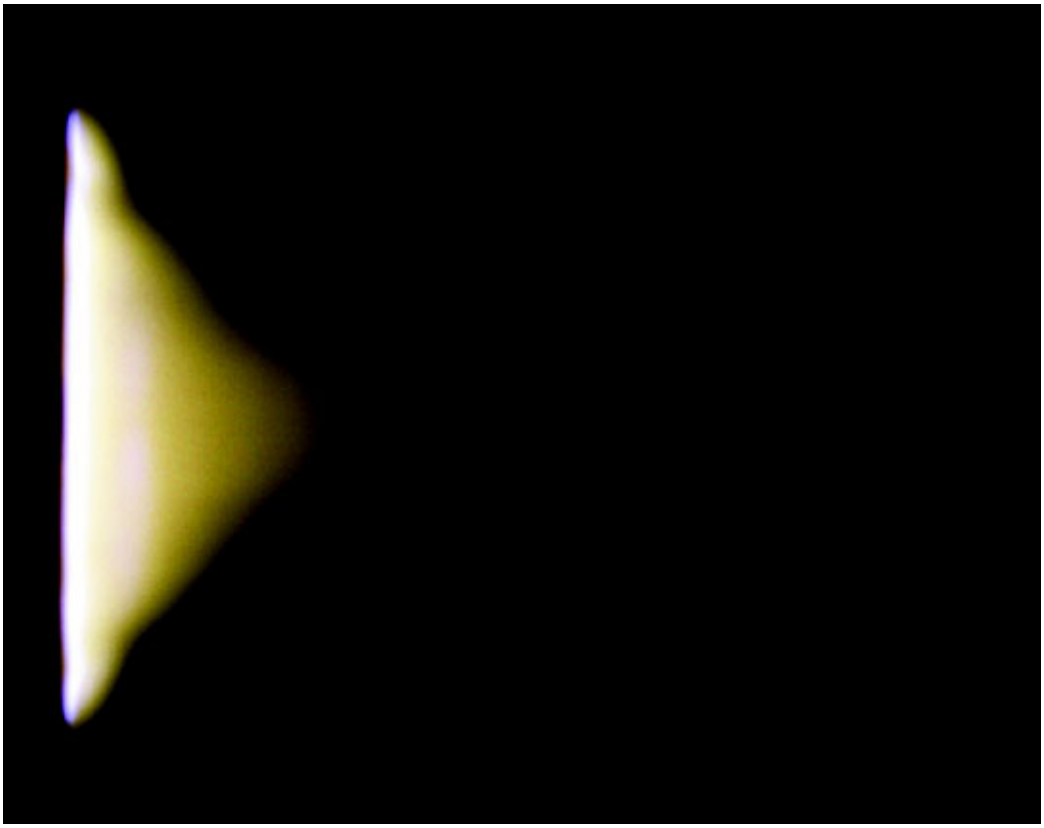

Fig. 7. Visualization of proboscis in air enriched with oxygen.

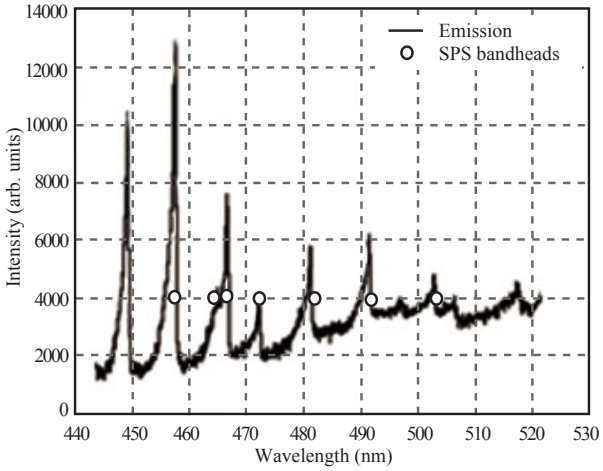

Fig. 8. Emission spectrum from the second plasmoid with a background suggestive of chemiluminescence.

electrical breakdown, but the field at interference maxima was high enough to generate plasmoids. Therefore, in this case, the surface plasma was eliminated but several bright, contracted plasmoids appeared. Although the pressure range for inception of plasmoids without surface plasma was narrow, in range of 65 to 75 torr, the result of this test indicates the possibility of eliminating the reflecting surface plasma layer.

D. Spatial Distribution of Plasma Parameters

D.1. End-on Observation

Microwave discharge excited by the X-band had a more stable pattern in comparison with the Ku-band. Questions arose immediately as to whether dark regions contain free electrons at all and therefore transmit microwave radiation. Our measurements show that dark regions emit Hydrogen Balmer lines, as well as emit most bands from the Second Positive and First Negative Systems. Therefore, electrons are present in the dark regions as well, but at a lower density. We measured electron density distribution between two bright spots and the result is given in fig. 9(a). The measurements were made using Stark profiles of the H_β line. Error bans indicate uncertainties in the evaluation procedure.

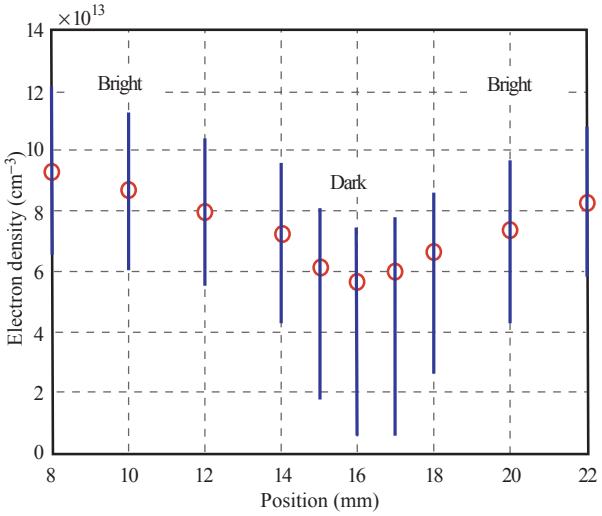

Fig. 9(a). Transverse distribution of electron density determined from end-on observations.

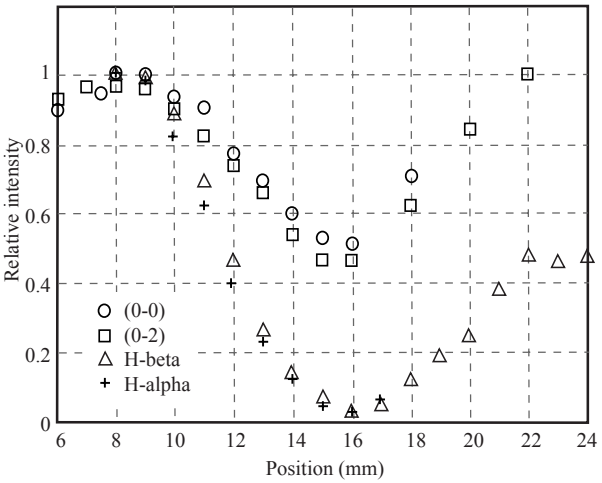

Fig. 9(b) Transverse distribution of the relative intensity of four different emission features.

In addition, we measured relative intensity distributions of hydrogen lines and the bandheads of the Second Positive System of nitrogen. These data are shown in fig. 9(b) and include the relative intensities of two bandheads, (0,0) at 337.13 nm and (0,2) at 380.49 nm, belonging to the SPS of molecular nitrogen and of two lines (H_β at 486.133 nm and H_α at 656.278 nm) belonging to the Balmer series of atomic hydrogen. Decrease of electron density in the dark spot, as seen in fig. 9(a), is consistent with the decrease of (ultraviolet) intensity of the nitrogen bandheads as shown in fig. 9(b). On the other hand, the intensity variation of the hydrogen lines (visible) is much more pronounced. Electron density near the maximum was derived from

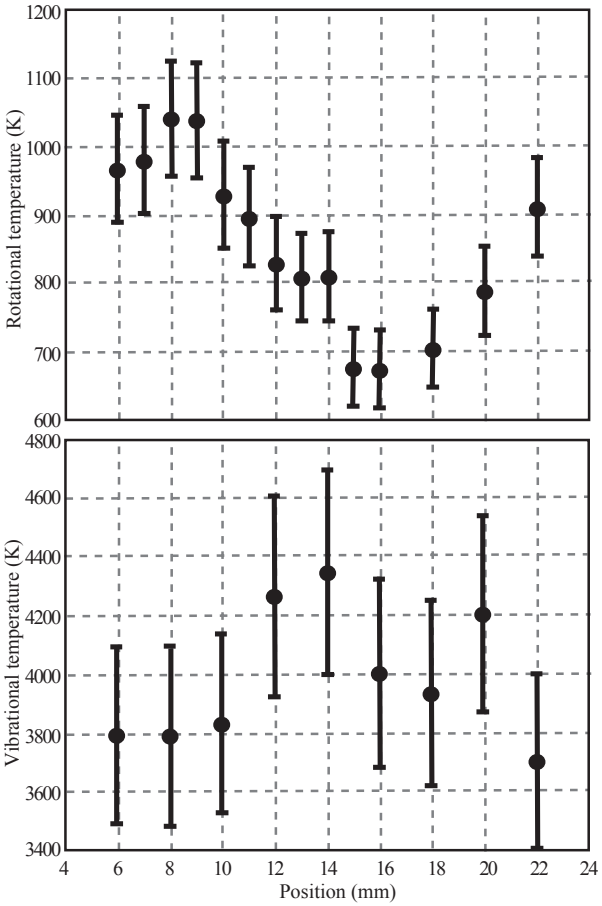

Fig. 10. Transverse rotational and vibrational temperatures determined from end-on spectral observations.

the Stark broadening of the H_β line by the fitting procedure (see appendix). Based on these data we can conclude that the extinction coefficient is reduced, but not enough to modify the structure of the discharge in the cell. Hence, we do not observe any effect from the surface discharge pattern on proboscis and standing wave plasmoids, except in the case of the discharge with the reflector where some plasmoids were wider and broken into fragments.

Transverse distributions of the rotational and the vibrational temperature are given in fig. 10. The temperatures were evaluated from end-on spectral observations between two central bright regions of the surface plasma pattern. The discharge was generated in air at 14 torr with the following X-band parameters: duration 3 μs, power 210 kW, and a repetition rate of 30 pps. Rotational temperature distribution shows the same pattern as the electron density. Vibrational temperature

distribution does not show the same behavior; its variations show the opposite trend of the distribution of electron density and rotational temperature. In both figures the error bars represent one standard deviation from linear fit. We note here that the line of sight in end-on observations crosses all plasma formations, proboscis, plasmoids, and the surface plasma and that all measured parameters are the average over that line-of-sight. Electron density and rotational temperature measurements are less affected by this spectral arrangement than the vibrational temperature measurements, which reflect the influence of plasmoid and proboscis that is more pronounced in the dark region. The dark region is more transparent for microwave radiation and therefore more microwave power is deposited locally into the corresponding parts of plasmoids.

D.2. Side-on Observation

Side-on measurements were initially planned for inspection of the self-absorption effects in spectral observations; however, the existence of self-absorption effects was not established. Two new interesting features were observed, and they justified the position-dependent observations in these two arrangements: (a) diffuse glow of relatively low intensity, protruding substantially into the cell volume (the proboscis), and (b) up to seven standing wave plasmoids. In Ku-band another pair of plasmoids were observed at and near the surface of the cell window, about 30 cm away from the model's surface.

Detailed electron density distribution through the surface plasma layer is given in fig. 11. These measurements were taken in air (no oxygen enrichment) with the reflector removed. An example of band emission at 337.13 nm is shown in fig. 12 as suggestive of a presence of substantial electron density in the proboscis. The spectrum was generated in room air at 10 torr with X-band parameters: duration 3 μs, power 210 kW, and a repetition rate of 30 pps. Electron density was measured using three methods. First, in the plasma layer, where Balmer line broadening is marginal but adequate, the electron density was obtained from the fitting procedure as an "absolute" value. Second, in the proboscis region the data are based on relative measurements of band intensities. Variation of the 337.13-nm band intensity was verified to be linear with electron density in the transition region from the surface discharge to the proboscis. The relative reduction of band intensity in the proboscis was evaluated and attributed to the relative reduction of electron density. The

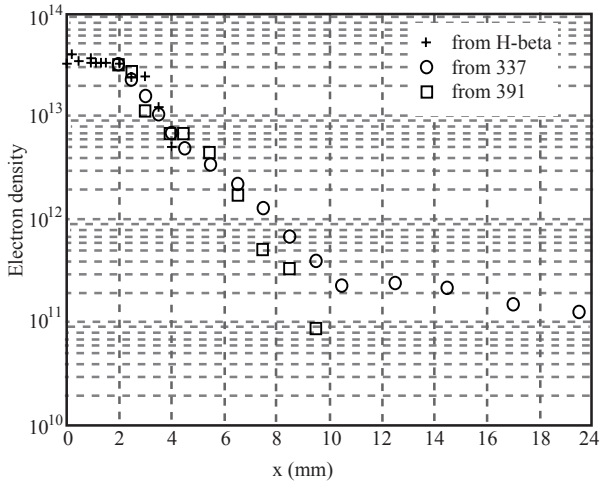

Fig. 11. Longitudinal electron density distribution in the surface plasma and proboscis, determined from H_β linewidth, N_2, and N_2^+ band intensities.

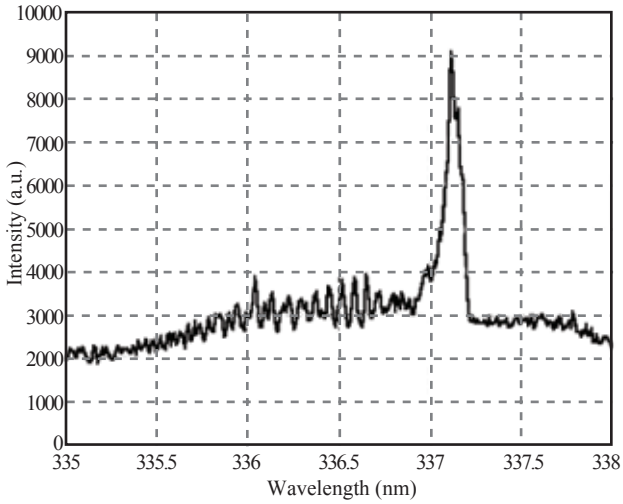

Fig. 12. Intensity of the (0,0) band at 337.13 nm in the proboscis region, 2.5 cm from the model.

technique is explained in the appendix together with an argument for the use of steady-state relation for this estimate. Third, in a similar manner, the variation of the 391.44-nm band with electron density in the transition region was established and the same trend was assumed to remain along the proboscis region.

Luminous structure observed at the aperture (see (fig. 4) seems to indicate that the surface plasma is

partially transparent to the microwaves, allowing their penetration into the cell space. Indeed, the existence of the proboscis, the plasmoid structure and our measurements give sufficient proof that the surface plasma transmits mostly through dark, low plasma density "holes."

Intensity of the (0-2) band of the C-B system is two orders of magnitude higher at the surface than in the proboscis indicating much higher population of the C states due to higher electron density. However, the rotational temperature of these states is comparable and even lower at the surface than at certain hot spots in the proboscis. The effect is more pronounced with Ku-band than with X-band.

The intensity of the 337.13-nm band strongly depends on the reduced electric field through the excitation rate coefficient [2,3]. Even though the measurements in these references are performed with pure nitrogen, we use their results to develop a quantitative understanding of the surface plasma, proboscis, and standing wave plasmoids. Reduction of the electric field by a factor of two leads to the reduction of the excitation coefficient by an order of magnitude. Therefore, the band intensity is not a useful indicator for electron density in the surface discharge region, which is about 2 mm wide and characterized by a steep decrease of the electric field due to reflection. In the proboscis region, reflectance is low and the reduction of the electric field is smaller. In addition, it can be assumed that this reduction is compensated by the increase of the field on the axis, which is due to the contraction of the microwave beam. The 391.44-nm band is not affected so much by the electric field, and it shows a similar trend as that of the 337.13-nm band in the region of 2 to 8 mm from the horn aperture.

With the reflector in place, a series of plasmoids are formed as illustrated in fig. 3. Side-on spectral measurements indicate that the electron density of the first few strong plasmoids in front of the horn is in the range of 10^{12} to 10^{13} cm^{-3}.

E. Discussion

The observed spatial pattern of plasmoids, which corresponds to the standing-wave radiation pattern in the near-field (Fresnel) regime, could have an interesting possibility for application in the experiments on volumetric plasma combustion.

When a reflector is placed in the beam at a distance corresponding to one half of a multiple of the microwave wavelength, a resonant linear cavity is formed and a standing microwave pattern is generated. A series of electric field maxima is formed at equally spaced positions inside the cavity. The series of plasmoids is formed practically at the same instant that the electric field maxima in the standing wave meet the breakdown condition, as shown in figs. 3 and 5. After breakdown, the plasma could be sustained with lower electric field levels. This standing wave plasmoid pattern represents a configuration that can provide volumetric energy deposition, which potentially can achieve the ignition condition simultaneously at a number of different locations.

In the near-field region, which is about 10-20 wavelengths long (fig. 6) the radial electric field distribution is narrowed and enhanced along the axis resulting in the "effective focusing." This phenomenon, partly visualized in figs. 3 and 7, contributes further to the field enhancement and excitation of plasmoids. Upon leaving the horn aperture, the microwave beam has a complex structure as the result of diffraction (fig. 6). The beam narrows to a minimum size at about 5 wavelengths from the horn. Further along the beam axis, it starts expanding to obtain the far-field (Fraunhofer) pattern.

Multiple peaks in the amplitude ripple at the aperture result in the formation of bright and dark spots on the surface of the horn, as observed in fig. 4. Bright spots are the signatures of high E/N surface plasma formations that develop a rather high electron density. Experimental time-averaged electron density at the bright spot (fig. 9(a)), consistent with calculations based on the theory outlined in ref. [9], is rather high and leads to a decrease in power transmission. Data shown in fig. 9(a) were taken with X-band microwaves, but a similar pattern was observed with Ku-band microwaves in which the electron density at the bright spots was slightly higher.

We note here that the values given in figs. 9 and 10 are averaged over the whole microwave pulse and also averaged over the line-of-sight that is through the surface plasma in the case of end-on observations. The induction period of the plasma, which is approximately 1 μs, could not be evaluated in full in these integrated measurements. This effect was observed only with the gated video camera without any spectral resolution, and in the time waveforms of forward and reflected microwave power. There was an interval in the microwave pulse, with a duration of about 0.5 μs, where the full forward power was achieved and the reflected power was negligible. This interval corresponded to a limited plasma pattern on the surface and the most intensive

plasmoid structure in the cell volume. However, in certain cases the plasmoid structure persisted and its intensity was increasing with the microwave pulse duration. Fully transmitted power in the first segment of the microwave pulse generated the plasmoid pattern, and the low transmitted power in the later segments was able to sustain and enhance the plasmoid structure.

The effect of averaging along the line of sight is more clearly seen in the bandhead intensity distribution (fig. 9(b)). Bandhead intensity is dependent on the product of the electron density, neutral number density, and the rate of excitation of the upper electronic state, which is strongly dependent on the electric field [2,3]. At the bright spot, the electron density is high, but average electric field is low due to low transmission, and the neutral density is low due to high temperature (fig. 10(a)). At the dark spot, electron density is low but electric field is high due to high transmission, and neutral density is high due to low temperature. Hence, the contrast is much less pronounced than in the case of hydrogen line intensities.

The nature and the role of the proboscis in the volumetric plasma formation is not yet completely clear. However, electron density of 10^{11} to 10^{12} cm^{-3} is high enough to open many processes of ion chemistry and produce a substantial density of radicals that could promote the ignition process and contribute to combustion.

F. Conclusion

Results of electron density measurements in the static cell are consistent with the electron density calculated in ref. [1] for a thin plasma situated on a bow shock in a Mach 6 tunnel. Maximum electron density in a bright spot of a surface plasma generated by X-band (210 kW microwave pulse, 3 μs duration) in air at 14 torr was 9×10^{13} cm^{-3} at a degree of ionization of 6×10^{-4}. An almost identical result was obtained in the cell using Ku-band (400 kW) at the same pressure and pulse duration.

Energy deposition into free flow by microwave-induced plasma is a promising method both for flow modification and combustion applications. We describe the plasma formation generated with a linear cavity in the near field of a microwave radiation beam. The diffuse plasma formation consists of three features: (1) standing-wave plasmoids distributed periodically along the microwave cavity axis, (2) the proboscis, a diffuse weakly ionized gas protruding along the beam, and (3) diffraction-patterned surface plasma. We characterized all three features by end-on and side-on spectroscopic observations and time-gated optical imaging.

We find the near-field plasmoid formation a potentially interesting form of energy deposition for volumetric ignition and combustion at low-density conditions. Plasmoids are generated in the first segment of microwave pulse, when surface plasma is still not fully formed and transmits almost full microwave power. They can be then sustained with a lower level of transmitted microwave power. Proboscis is the weakly ionized gas around the plasmoids containing still a rather high degree of ionization (10^{-6} to 10^{-5}).

G. Appendix

G.1. Electron Density

Electron density is determined from Stark broadening of the H_β line following the standard procedure based on the work of Vidal, Cooper, and Smith [10], and further developed by Kelleher [11] for relatively large electron densities. It has been extensively used for electron density diagnostics in partially ionized air [12–15]. However, Goode and Deavor [16] have pointed out that the curve-fitting approach to evaluation of electron density is expected to be more accurate than the single-point procedure of ref. [11] at relatively low electron densities. In direct comparisons of the two approaches, Goode and Deavor's approach produces values of electron density several times lower than the standard procedure. At electron densities in the range of 10^{13} cm^{-3}, the discrepancy may be even higher. On the other hand, it is possible to obtain experimentally the H_β profile in this electron density range. We still consider the Goode and Deavor technique valuable and decided to use it in this work.

At an even lower electron density, in the proboscis region, electron density could not be determined from Stark broadening of Hydrogen Balmer lines. However, the emission band of the $C^3\Pi_u \rightarrow B^3\Pi_g$ system of molecular nitrogen could be seen at every position in the discharge structure (figs. 11 and 12). The simplified kinetic model of the upper state, $C^3\Pi_u$ (v = 0), consists of populating this state by direct electron excitation, depopulating by radiative transition into $B^3\Pi_g$ (v = 0), and quenching in the collisions with ground state molecules. If we assume a steady-state population of the upper state, we could obtain a linear relation between the 337.13-nm band intensity and electron density, $I\,(337.13\text{ nm}) \approx N_C \approx N_e$ at constant pressure and constant electric field (ref. [3]). This condition applies for very long pulses where the steady state is achieved.

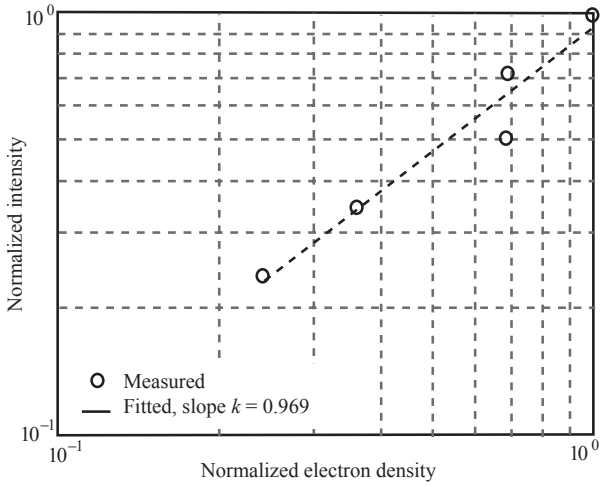

Fig. 13. Linear relation between electron density and the (0,0) band intensity of N_2 SPS.

We tested the linear relationship between the intensity of the 337.13-nm band and the electron density in the relatively narrow region in and around the surface discharge where Stark broadening of the H_β line could still be measured. At several various conditions at constant pressure, the plots of the band intensity versus electron density on a logarithmic scale have shown the slope corresponding to the exponent value between 0.96 and 1.05 (fig. 13). The discharge in fig. 13 was generated in room air at 10 torr with X-band parameters: duration 3 μs, pulse power 210 kW, and a repetition rate of 30 pps. Different values of the electron density were obtained by varying the measurement position in the plasma as seen in fig. 11 from 2 to 4 mm. Therefore, we concluded that the relation is indeed linear. Hence the intensity of the 337.13-nm band seems to be a good candidate for estimating electron density by assuming that the linear relationship can be extrapolated to a low density range.

G.2. Rotational and Vibrational Temperature

Rotational temperatures were measured from the rotational spectra of the $C^3\Pi_u \rightarrow B^3\Pi_g$ Second Positive System of molecular nitrogen. The spectra consist of triple-headed bands, all degraded to shorter wavelengths. The three branches are usually labeled P, Q, and R. Further, P and R branches are split into three subbranches, and Q branch is split into two. In most cases, we used the 380.49-nm (0-2) band because it exhibited the best resolved R branch spectra and has been preferably used for determination of rotational temperature. Relatively high rotational quantum numbers, typically from J = 18 to J = 27, were used in generating a Boltzmann plot for the intensity of the lines belonging to R branch. The term values for R branch are given by Herzberg [17], and the corresponding rotational constants were compiled using ref. [18]. The slope of the Boltzmann plot is remarkably uniform at the given pressure, and the evaluated temperature varies within ±3%.

We have limited vibrational analysis to the relative band intensity of various bands belonging to the Second Positive System. Having in mind that the pulse duration was not more than 3 μs, and that the analysis was limited to three to five bands in each sequence, we should not be able to generalize the assumption of the $v - v$ and $v - T$ equilibriums. However, in search for an additional parameter for characterization of microwave discharge we are introducing the effective vibrational temperature, assuming a Boltzmann factor is applicable to the limited number of the observed vibrational states. Frank-Condon factors were taken from ref. [19]; the energy factors of vibrational levels and the molecular constants for Second Positive System were taken from ref. [20]. Horizontal distribution of vibrational temperature was based on the data for the sequence $\Delta v = +1$ (1-0, 2-1, 3-2, 4-3) of the Second Positive System of N_2 at 315.93, 313.6, 311.67, and 310.4 nm. These measurements were confirmed at $\Delta v = 0, -2, -3, -4, -5$, and -6 with relatively low scatter of vibrational temperature data.

Acknowledgments

We wish to thank W. E. Lipford for his assistance in setting up the apparatus and in taking the data. The use of trademarks or manufacturers' names in this paper is for accurate reporting and does not constitute an official endorsement, either expressed or implied, by the National Aeronautics and Space Administration.

References

[1] R. J. Exton, R. J. Balla, B. Shirinzadeh, G. J. Brauckmann, G. C. Herring, W. C. Kelliher, J. Fugitt, C. J. Lazard, and K. V. Khodataev, Phys. Plasmas **8** (2001) 5013–5017.

[2] F. Cramarosa, G. Ferraro, and E. Molinari, JQSRT **14** (1974) 419–436.

[3] S. D. Popa, J. Phys. D: Appl. Phys. **29** (1996) 416–418.

[4] F. Mako, J. A. Pasour, C. W. Robertson, and R. Lucey, Rev. Sci. Instrum., **55** (1984) 712–715.

[5] S. Silver, Ed., Microwave Antenna Theory and Design (Dover Publ., New York 1965) p. 173.

[6] M. Ardon, Oxygen (W. A. Benjamin, New York 1965) pp. 13–17.

[7] G. A. Askar'yan, G. M. Batanov, S. I. Gritsinin, I. A. Kossyi, and A. Yu. Kostinskii, Sov. Phys. Tech. Phys. **35** (1990) 1275–1280.

[8] Y. Kolesnichenko et al., Partner Project 1779p, Final Report to European Office of Aerospace Research and Development, April 2001.

[9] K. V. Khodataev and B. R. Gorelik, Plasma Physics Reports, **23** (1997) 215–224.

[10] C. R. Vidal, J. Cooper, and E. W. Smith, Astrophys. J. Suppl. Series No. 214, **25** (1973) 37–136.

[11] D. E. Kelleher, JQSRT, **25** (1981) 191–220.

[12] C. Thomsen and V. Helbig, Spectrochimica Acta, **46B** (1991) 1215–1225.

[13] S. Jovičević, M. Ivković, Z. Pavlović, and N. Konjević, Spectrochimica Acta **55B** (2000) 1879–1893.

[14] C. O. Laux, Ph. D. Thesis, Stanford University (1993).

[15] L. Yu, Ph. D. Thesis, Stanford University (2001).

[16] S. R. Goode and J. P. Deavor, Spectrochimica Acta, **39B** (1984) 813–818.

[17] G. Herzberg, Molecular Spectra and Molecular Structure, I: Spectra of Diatomic Molecules (New York: Van Nostrand, 1950) pp. 233-235.

[18] A. Lofthus and H. P. Krupenie, The spectrum of Molecular Nitrogen, J. Phys. Chem. Ref. Data, **6** (1977) p. 242–244 (1977).

[19] G. Hartmann and P. C. Johnson, J. Phys. B: Atom. Molec. Phys. **11** (1978) 1597–1612.

[20] R. R. Laher and F. R. Gilmore, J. Phys. Chem. Ref. Data **20** (1991) 685–712.